Journal of
Applied
Crystallography
ISSN 0021-8898

Received 18 April 2005
Accepted 14 June 2005

Application of *in situ* vapor sorption small-angle neutron scattering (SANS) to semicrystalline polymers: vapor pathway and structure evolution in semicrystalline linear polyethylene

Man-Ho Kim[a,b]* and Charles J. Glinka[a]

[a]NIST, Center for Neutron Research, Gaithersburg, MD 20899, USA, and [b]MSE, University of Maryland, College Park, MD 20742, USA. Correspondence e-mail: man-ho.kim@nist.gov

SANS has not been successfully applied to study the structure of semicrystalline polyolefins without deuterated polymers because of the fundamental limitation of negligible contrast between the crystalline and amorphous phases in spite of the mass density difference. The proposed *in situ* vapor sorption SANS technique circumvents this limitation and enables structural changes to be studied quantitatively with sorption of a contrast-generating vapor. The results verify the long-standing assumption that vapor selectively diffuses into the amorphous regions of semicrystalline polyethylenes. The proposed technique makes it possible to correlate the structure, sorption isotherm and diffusion coefficient, which is not possible using conventional gravimetric methods.

1. Introduction

Polyolefins have been studied extensively since the 1950s. Polyethylene and other stereo-regular polyolefins are semicrystalline materials that always contain an amorphous fraction in the crystallized system. Crystalline structure, crystallization kinetics (Mandelkern, 2004) and morphology are important for understanding the material's properties. Most of these have been studied with small-angle (SAXS) and wide-angle (WAXS) X-ray scattering, small-angle light scattering (SALS), other radiation, or micro-spectroscopic methods, because the crystallized polyolefins have sufficient electron density difference or polarizability. SAXS has been used to understand the structure of lamellae, melting (Kim *et al.*, 2000; Schmidtke *et al.*, 1997; Hsiao *et al.*, 1993) and the crystallization behavior (Loo *et al.*, 2001), while SALS has been applied to study the spherulite morphology, size and deformation (Akpalu *et al.*, 1999). On the other hand, SANS has unique features like strong penetration, contrast variation and relative ease of obtaining absolute intensity. Like other scattering techniques, SANS requires contrast, the so-called neutron scattering length density (SLD) difference. Some polymeric materials have natural contrast, while for others a mixture of protonated and deuterated polymers is necessary to produce contrast for SANS. The benefit of the SLD difference between hydrogen ($b_H = -3.73$ fm) and deuterium ($b_D = 6.67$ fm) allows SANS to be a valuable tool for studying melt phase behavior, single chain conformation and its distribution in crystalline phases (Wignall, 2004; Schelten *et al.*, 1976; Stamm *et al.*, 1979; Guttman *et al.*, 1981), *n*-paraffin deposition and inhibitors (Leube *et al.*, 2000), and blends (Agamalian *et al.*, 1999; Lee *et al.*, 2003), and so on, although the deuterated and hydrogenated polymers have different thermodynamics and crystallization kinetics.

One of the purposes of this study is to demonstrate a way to apply SANS to semicrystalline polyolefins without using deuterated polymers by the *in situ* vapor sorption method. There have been a couple of related studies using water vapor to enhance scattering contrast in cellulose (Fischer *et al.*, 1978) and in Nylon 6[1] (Murthy *et al.*, 1989, 1998) at saturated relative humidity. These systems have strong secondary interactions, such as hydrogen bonding between polymers and moisture. To our knowledge, the contrast-enhancement technique by *in situ* vapor sorption has not been applied to semicrystalline polymers, especially non-polar polymers such as polyolefins. Compared with polar polyamides, the non-polar polyolefins are a different kind of semicrystalline polymer, which have only a weak secondary force, the van der Waals dispersion force, between the chains. It has been reasonably assumed that organic molecules selectively diffuse into the amorphous phase in semicrystalline polymers, and (indirectly) estimated from the decrease of the diffusion rate with crystallinity (Rogers *et al.*, 1959; Weinkauf, 1990; Doong & Ho, 1991; Castro *et al.*, 1987; Paricaud *et al.*, 2004), although there are some exceptions. Changes in nanoscale structure with sorption time, however, have not been determined quantitatively, although attempts have been made to explain diffusion/sorption phenomena with concepts such as cross-section area, free volume, and chain flexibility of the amorphous phase.

[1] Certain commercial equipment, instruments or materials are identified in this paper to foster understanding. Such identification does not imply recommendation or endorsement by the National Institute of Standards and Technology, nor does it imply that the materials or equipment identified are necessarily the best available for the purpose.

The negligible SANS scattering of semicrystalline polymers that is a disadvantage for studying the crystalline structure can be an advantage in identifying a vapor diffusion pathway in semicrystalline polymers. If SANS intensity related to the lamellar structure appears during sorption of a contrast-generating vapor, this implies that the contrast-generating vapor is preferentially absorbed into one of the phases, which will allow us to track structure evolution quantitatively with sorption time. The *in situ* vapor sorption/SANS and wide-angle X-ray scattering (WAXS) data presented here demonstrate that the vapor diffusion pathway in semicrystalline polyolefin polymers is indeed the amorphous region as shown in the Nylon-6/moisture system (Murthy *et al.*, 1989, 1998). The technique of following the development of scattering contrast with sorption time is shown to be valuable for understanding diffusion and sorption behavior from a structural point of view. A relationship between vapor sorption and structure of polyolefins would be valuable for developing food packaging barriers, polyolefin polymerization processing, and membrane morphology. For example, in the polyolefin industry, it has been known that olefin monomers grow and crystallize on the active surfaces of porous heterogeneous catalysts. Olefin monomers penetrate into the growing semicrystalline polymer particles surrounding the catalyst and reach the interface between the catalyst and polymer, which allows the polymerization reaction to continue (Hutchinson & Ray, 1990; Mckenna, 1998). Gravimetric methods have also been used to study sorption kinetics by monitoring changes in sample mass with sorption time. When sorption kinetics are compared with changes in the structure parameters, such as long spacing, radius of gyration, lamellar thickness *etc.*, a better understanding of the sorption isotherm and diffusion kinetics is likely to emerge. It is also of practical interest to understand polymer semicrystalline structure under a vapor environment because most materials (for example, barrier polymers) in our life are exposed to many kinds of vapors, including moisture, and vapor affects the end-product material properties.

The purpose of this study is (i) to demonstrate the effectiveness of vapor sorption for increasing scattering contrast in SANS measurements of semicrystalline polyolefins, (ii) to find the diffusion pathway of hydrocarbon vapor in semicrystalline polyethylene, and (iii) to follow the structure evolution[2] quantitatively with sorption time. For this purpose, an *in situ* vapor sorption apparatus for SANS with fine control of small amounts of contrast-generating organic vapor was built.

2. Experimental

The *in situ* sorption apparatus used in this study has two modes of operation. The vapor above a solvent reservoir can be admitted to an evacuated sample cell and monitored to achieve a preset fraction of the solvent's saturated vapor pressure. Alternatively, vapor-saturated carrier gas, or a mixture of saturated and dry carrier gas, can be flowed continuously through the sample cell. A detailed description of this apparatus will be given elsewhere (Kim *et al.*, 2005). In this study, the latter method was used.

Two films, each with a thickness of 0.100 (1) mm, composed of linear polyethylene (each with weight- and number-average molar mass of M_w = 101.3 kg mol^{-1} and M_n = 53.9 kg mol^{-1}, respectively) were prepared on a hydraulic press at a melt temperature of 443 K. One (PEqch, density ρ = 0.9313 g cm^{-3}) was non-isothermally crystallized for 30 min in water at $\sim$296 K by quenching the pressed melt. The other (PE110, ρ = 0.9667 g cm^{-3}) was isothermally crystallized for 1.5 days at 383.0 $\pm$ 0.5 K by transferring the melt to an oven at a pre-set temperature. Density was measured in a density gradient column with a mixture of methanol/ethylene glycol at 296 K. The SANS experiment was performed on a 30 m pin-hole collimation instrument at the NIST Center for Neutron Research. The sample-to-detector distance was 7.0 m for PE110 and 4.7 m for PEqch, with an 8.09 Å wavelength with $\Delta\lambda/\lambda \simeq 11\%$. The transmission of the dry PE110 sample was 90% for a volume crystallinity of φ_c = 78%, and was 85% for PEqch with φ_c = 54%. Volume crystallinity, $\varphi_c = (\rho - \rho_a)/(\rho_c - \rho_a)$, was estimated from the measured sample density (ρ), the orthorhombic crystalline density (ρ_c = 1.0 g cm^{-3}) and the ideal amorphous phase density ($\rho_a \simeq 0.85$ g cm^{-3}) of polyethylene. The transmission of wet samples was 1 or 2% lower.

3. Results and discussion

Fig. 1(*a*) shows the SANS data for dry PE110 and dry PEqch. There is no peak from the crystalline/amorphous lamellar structure, whereas a strong peak is seen in the corresponding SAXS data in Fig. 1(*b*). It is worthwhile discussing the reason for this here. All small-angle scattering phenomena require a kind of contrast depending on the radiation source:

$$I(q) \propto \varphi(1-\varphi)(\Delta\mathrm{SLD})^2 K, \qquad (1)$$

where K represents the form factor or/and structure factor whose expression depends on the volume fraction, φ, the polydispersity and the orientation of the scatterers.

In small-angle scattering, contrast is defined as the squared difference, $(\Delta\mathrm{SLD})^2$, of the coherent scattering length densities (SLD) between phases or domains in a material. The SLD is given by $\mathrm{SLD}_{\mathrm{neutron}} = \left(\sum_i^n b_i\right)/V$ for neutrons, and $\mathrm{SLD}_{\text{X-ray}} = \left(r_e \sum_i Z_i\right)/V$ for X-rays, where b_i is the bound coherent scattering length of atomic species i, r_e is the classical radius of the electron (= 2.817940 $\times$ 10^{-13} cm), Z_i the number of electrons (*i.e.* atomic number) of the atom i in a repeating unit of the polymer chain. $1/V$ (cm^{-1}) is the number density given by $N_A\rho/M_w$, where N_A is Avogadro's number (6.022 $\times$ 10^{23} mol^{-1}), ρ is the mass density (g cm^{-3}), and M_w is the molar mass (g mol^{-1}) of a repeating unit of a polymer chain. The contrast between the crystalline and amorphous phases of a semicrystalline polymer is, therefore,

[2] Structure evolution refers to both the appearance of the hidden structure and changes in the structure with sorption time of the contrast-generating vapor.

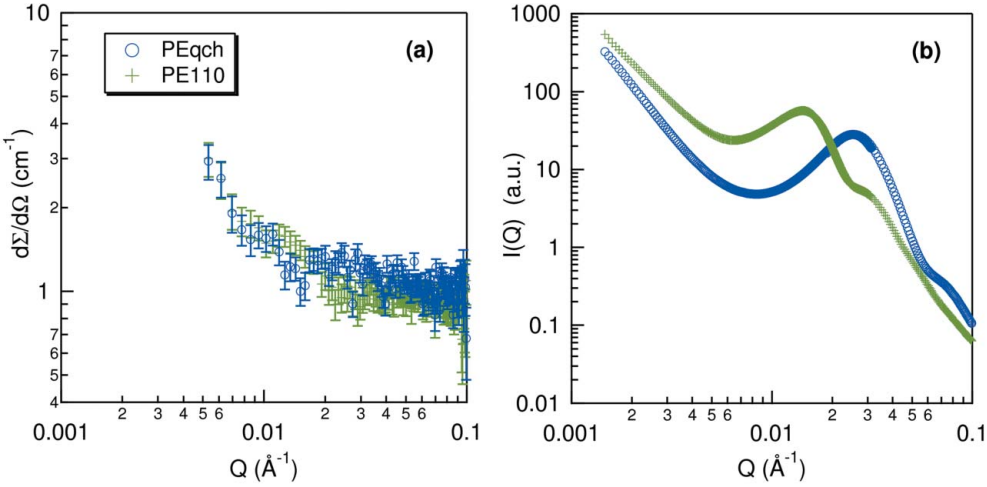

Figure 1
(*a*) SANS total cross section (*i.e.* absolute intensity) of the dry polyethylenes: PEqch and PE110 with 54% and 78% degree of volume crystallinity; (*b*) corresponding synchrotron SAXS (in arbitrary units). Both SANS and SAXS intensities were measured with a sample thickness of 100 ± 1 µm at room temperature using pin-hole collimation.

Table 1
X-ray and neutron contrast $(\Delta\text{SLD})^2$ (cm^{-4}) between the crystalline, amorphous, d_{14}-hexane bulk liquid and vapor-saturated regions of the linear polyethylene samples.

	$(\Delta\text{SLD})^2_{\text{X-ray}}$	$(\Delta\text{SLD})^2_{\text{Neutron}}$	$(\Delta\text{SLD})^2_{C_6D_{14}/\text{Neutron}}$	
			Bulk liquid C_6D_{14}	$\varphi_{C_6D_{14}}(t)$†
PEqch	6.19×10^{19}	8.43×10^{16}	4.19×10^{21}	8.21×10^{19}
PE110	1.28×10^{20}	1.74×10^{17}	4.20×10^{21}	4.20×10^{19}

† Estimated from equation (4) with 14% and 10% $\varphi_{C_6D_{14}}(t)$ for PEqch and PE110, respectively, assuming $\varphi_{C_6D_{14}}(t) \cong \Delta L/L$.

$$\Delta\text{SLD} = \left(\sum_i^n b_i\right)\Big/V_c - \left(\sum_i^n b_i\right)\Big/V_c = \text{SLD}_c(1 - \rho_a/\rho_c), \quad (2)$$

where the subscripts c and a refer to the crystalline and amorphous phases, respectively. Hence the ratio of the contrast factors for neutrons and X-rays is

$$(\Delta\text{SLD})^2_{\text{Neutron}}/(\Delta\text{SLD})^2_{\text{X-ray}} = \left(\sum_i^n b_i\right)^2 \Big/ \left(r_e \sum_i Z_i\right)^2. \quad (3)$$

The $(\Delta\text{SLD})^2$ of polyethylenes, assuming an ideal two-phase model, is given in Table 1 for both neutrons and X-rays. $(\Delta\text{SLD})^2_{\text{Neutron}}$ is approximately three orders of magnitude smaller than $(\Delta\text{SLD})^2_{\text{X-ray}}$, in spite of the mass density difference between the crystalline and amorphous phases. Low contrast in SANS in Fig. 1(*a*) is due to the near cancellation, $\left(\sum_i^n b_i\right)^2 = (b_C + 2b_H)^2 \simeq 0$, of neutron scattering lengths between carbon ($b_C = 6.646$ fm) and two hydrogen ($2b_H = -7.478$ fm) atoms composing polyethylene, which causes near negligible SANS scattering. This fundamental limitation of low contrast in SANS for the semicrystalline system can be overcome if a particular phase can be selectively wetted with a contrast-generating vapor. This is demonstrated in Fig. 2. Once a small amount of d_{14}-hexane (C_6D_{14}) vapor penetrates the sample, the isotropic scattering signal (circular pattern) appears within a few minutes, as shown in the two-dimensional image. The contour of the two-dimensional image becomes more distinct as wetting time increases. The corresponding one-dimensional plot (*i.e.* intensity *versus* q) shows that the intensity around $q \simeq 0.013$ Å^{-1} increases and simultaneously a broad bump appears around $q \simeq 0.027$ Å^{-1} with increasing wetting time. If we denote the volume fraction of condensed d_{14}-hexane in the amorphous phase by $\varphi_{C_6D_{14}}(t)$, such that $\varphi_a + \varphi_{C_6D_{14}}(t) = 1$, where φ_a is the volume fraction of amorphous polymer in the amorphous phase and t is sorption time, then the expression for contrast, equation (1), can be written approximately as

$$(\Delta\text{SLD})^2 \cong [\varphi_{C_6D_{14}}(t)(\text{SLD}_c - \text{SLD}_{C_6D_{14}})]^2, \quad (4)$$

where $\text{SLD}_{C_6D_{14}}$ is the scattering length density of bulk liquid d_{14}-hexane. The contrast, $(\Delta\text{SLD})^2_{C_6D_{14}/\text{Neutron}}$, between the crystalline phase and the bulk liquid C_6D_{14} is of the order of 10^4 larger than $(\Delta\text{SLD})^2_{\text{Neutron}}$ between the crystalline and the amorphous phase for neutrons, so that even rather small values of $\varphi_{C_6D_{14}}(t)$ produce considerable contrast, as seen in Table 1. Equation (4) emphasizes that the change in scattering intensity serves to monitor directly the amount of condensate in the sample.

Although Fig. 2 demonstrates that one phase is selectively wetted by the d_{14}-hexane vapor, SANS does not identify directly which phase the vapor wets because either case will generate contrast. To determine the location of the vapor in semicrystalline polymers, we rely on the following logical argument, assuming an ideal two-phase system: the ideal density of the orthorhombic crystalline phase in the lamellae is higher than that of the amorphous phase. This suggests that the amorphous phase has more unoccupied volume (*i.e.* free volume) and more flexible chains than the more tightly packed crystalline phase. Thus vapor has more chance to penetrate into the flexible amorphous region and to condense in the free volume. In addition, the unit-cell dimension would expand if

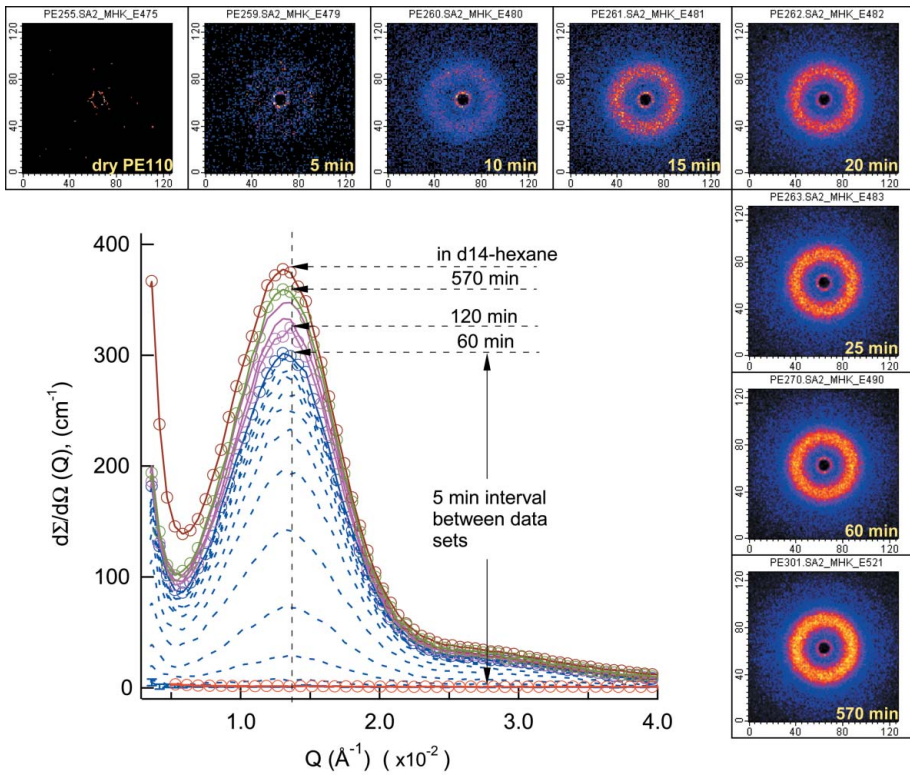

Figure 2
Structure evolution of PE110 with vapor (d_{14}-hexane) sorption. The SANS intensity profile and selected two-dimensional image were collected as a function of sorption time by wetting the sample with the contrast-generating vapor using an N_2 carrier gas [flow rate 0.5 standard cm^3 min^{-1} (= 1.7 × 10^{-8} m^3 s^{-1})] passing through a solvent reservoir from the upstream side. The carrier gas leaving the bubbler was assumed to be saturated. Intensity was recorded with a 5 min SANS run time interval from the initial stage. The error bars in the one-dimensional plot were removed for clarity. The error ranges are within the open-circle symbols.

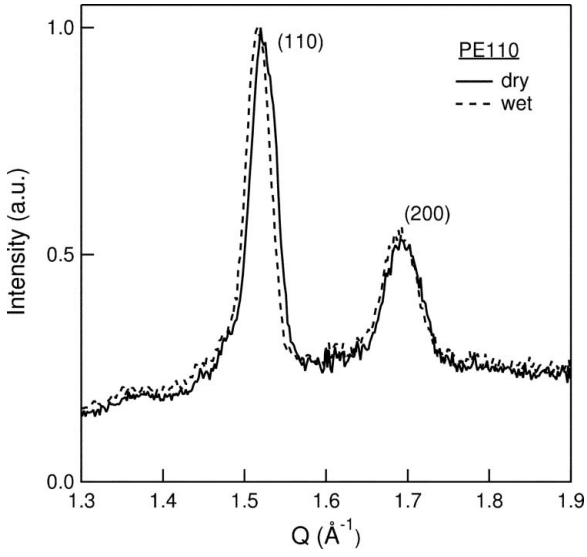

Figure 3
WAXS profiles of the fresh and *n*-hexane-saturated PE110 obtained using Cu $K\alpha$ radiation with a wavelength λ of 1.54 Å and a position-sensitive detector. The sample was wetted for 10 min with an *n*-hexane-soaked paper towel on the X-ray sample stage. There is a small difference between dry and wet PE110, as much as $Q = 3.896 \times 10^{-3}$ Å^{-1} with a corresponding *d*-spacing difference $\Delta d = 0.01$ Å, based on the 110 reflection ($Q = 1.520$ Å^{-1}) of orthorhombic symmetry.

the vapor penetrated into the crystalline phase. The WAXS intensity (Fig. 3) for the dry and solvent-saturated PE110 shows almost identical peak positions with a small deviation, $\Delta q/q < 0.3\%$, in the 110 peak, which corresponds to a *d*-spacing change of $\Delta d \simeq 0.01$ Å. The *in situ* vapor sorption/SANS and independent WAXS results clearly demonstrate that vapor is selectively absorbed predominantly within the amorphous phase of the semicrystalline polyethylene, and that the crystalline structure is not significantly altered.

Figs. 2 and 3 are the experimental evidence demonstrating selective vapor sorption in the amorphous regions of the polyethylene samples. Intensities of both PE110 and PEqch increase with sorption time with little change in the shape of the isotropic scattering profile. In Fig. 2, there is no indication of any structural modification of PE110 during wetting. The peaks were fitted with a Lorentzian function and the results are shown in Fig. 4. During sorption in PE110, the long period $L = (2\pi/q_{peak})$, which is the repeat distance of the crystalline and amorphous phases in the lamellar stack, increases by as much as approximately 8 Å, while L of PEqch increases by 17 Å after an induction time of around 10 min. Expansion of the long period is $\Delta L/L = 8/472 \simeq 2\%$ for the PE110 and $\Delta L/L = 17/268 \simeq 6\%$ for PEqch. This implies that the poorly crystallized PEqch may have more free volume than the PE110. (This difference in $\Delta L/L$ supports our understanding that the PEqch, with a higher amorphous volume fraction than PE110, also has more free volume.) Since the vapor is selectively absorbed in the amorphous phase as justified before, the increase of L is due to an expansion of the amorphous phase only. The degree of expansion of the amorphous phase, $\Delta l_a/l_a$, is $10/104 \simeq 10\%$ for PE110, and $\Delta l_a/l_a = 17/123 \simeq 14\%$ for PEqch, where the averaged crystalline and amorphous phase thickness of the dry samples was estimated from $l_c = L\varphi_c$ and $l_a = L(1 - \varphi_c)$, respectively, assuming a two-phase model. For saturated samples, the amorphous phase thickness $l_a(\mathrm{sat})$ was obtained from L of the saturated sample and l_c of the dry sample, $l_a(\mathrm{sat}) = L(\mathrm{sat}) - l_c$, where l_c is the same as that of the saturated sample; $l_c = l_c(\mathrm{sat})$, due to impermeability of vapor into the crystalline phase.

In Fig. 5 we compare in greater detail the SANS data from the vapor-saturated PE110 sample with synchrotron SAXS data for a dry PE110 sample from the same batch of starting material. For the comparison, the peak intensities were matched in height and position. The peak profiles are nearly identical. The only difference is that the SANS data show a

deeper valley near $q = 0.0014$ Å^{-1} than the USAXS/SAXS data. This result clearly shows that the *in situ* sorption technique introduces scattering contrast without changing the underlying phase structure.

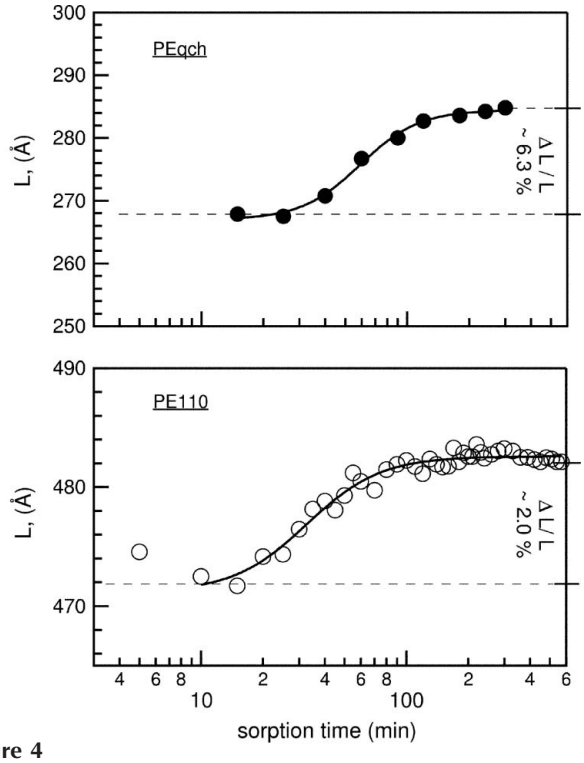

Figure 4
Long period (L, Å) of PEqch and PE110 with vapor sorption time. The overall change of L for the isothermally crystallized PE110 is around 2%, while the rapidly crystallized PEqch shows an increase of around 6%. Both PEs show an induction time before L starts to increase. The L within the induction time represents the L of the dry sample.

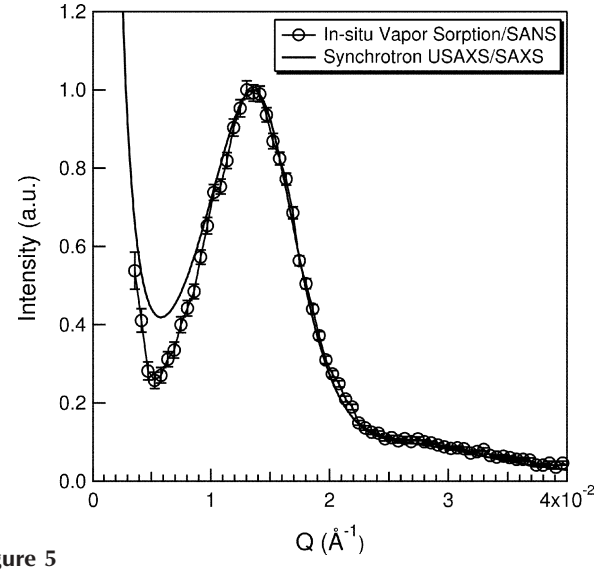

Figure 5
Comparison of *in situ* vapor sorption/SANS (open circles) and USAXS/SAXS (solid line). The SANS profile (10 min sorption and 5 min SANS run) is of one of the intensities shown in Fig. 3, and the USAXS is from dry PE110. The intensity was matched in the peak height and peak position. The SAXS peak was shifted to the SANS peak by $\sim 1.2 \times 10^{-3}$ Å.

4. Conclusions

The fundamental limitation of negligible neutron scattering contrast between the crystalline and amorphous phases in semicrystalline polymers can be overcome with the *in situ* vapor sorption technique. In the early stage of vapor sorption, sufficient contrast develops to provide the same structural information as X-ray measurements on dry samples. The long period expands slightly (less than 10%) in inverse proportion to the degree of crystallinity, due to swelling of the amorphous region. The quality of the data is comparable with that of synchrotron SAXS data based on the FWHM (full width at half-maximum) and degree of contrast. The results of *in situ* vapor sorption/SANS and WAXS demonstrate that contrast-generating vapor selectively diffuses into the amorphous phase even if there is no strong interaction force between the vapor and the polymer chains. The *in situ* vapor sorption/SANS method can be used to study sorption kinetics as an alternative to gravimetric methods. This makes it possible to correlate the sorption/diffusion behavior with structure evolution during sorption, and to extract a diffusion coefficient and interaction parameter. Contrast variation by selective *in situ* vapor sorption is expected to enhance considerably the application of SANS to the study of semicrystalline polymers, packaging barriers and membranes.

This work is based on activities supported by NSF (DMR-9986442). We wish to thank J. David Londono for the synchrotron SAXS experiment and Nitash P. Balsara and Megan Ruegg for density measurements. Synchrotron SAXS work was performed at the DuPont–Northwestern–Dow Collaborative Access Team (DND-CAT) Synchrotron Research Center located at Sector 5 of the Advanced Photon Source. DND-CAT is supported by E. I. DuPont de Nemours & Co., The Dow Chemical Company, the US National Science Foundation, through Grant DMR-9304725, and the State of Illinois, through the Department of Commerce and the Board of Higher Education Grant IBHE HECA NWU 96. Use of the Advanced Photon Source was supported by the US Department of Energy, Basic Energy Sciences, Office of Energy Research, under Contract No. W-31-102-Eng-38.

References

Agamalian, M., Alamo, R. G., Kim, M.-H., Londono, J. D., Mandelkern, L. & Wignall, G. D. (1999). *Macromolecules*, **32**, 3093–3096.

Akpalu, Y., Kielhorn, L., Hsiao, B. S., Stein, R. S., Russell, T. P., van Egmond, J. & Muthukumar, M. (1999). *Macromolecules*, **32**, 765–770.

Castro, E. F., Gonzo, E. E. & Gottifredi, J. C. (1987). *J. Membrane Sci.* **31**, 235–248.

Doong, S. J. & Ho, W. S. W. (1991). *Ind. Eng. Chem. Res.* **30**, 1351–1361.

Fischer, E. W., Herchenroder, P., Manley, R. St J. & Stamm, M. (1978). *Macromolecules*, **11**, 213–217.

Guttman, C. M., DiMarzio, E. A. & Hoffman, J. D. (1981). *Polymer*, **22**, 1466–1479.

Hsiao, B. S., Gardne, K. H., Wu, D. Q. & Chu, B. (1993). *Polymer*, **34**, 3996–4003.
Hutchinson, R. A. & Ray, W. H. (1990). *J. Appl. Polym. Sci.* **41**, 51–81.
Kim, M.-H., Glinka, C. J. & Carter, R. N. (2005). *Rev. Sci. Instrum.* Submitted.
Kim, M.-H., Phillips, P. J. & Lin, J. S. (2000). *J. Polym. Sci. Part B Polym. Phys.* **38**, 154–170.
Lee, J. H., Ruegg, M. L., Balsara, N. P., Samuel, Y. Z., Gido, P., Krishnamoorti, R. & Kim, M.-H. (2003). *Macromolecules*, **36**, 6537–6548.
Leube, W., Monkenbusch, M., Schneiders, D., Richter, D., Adamson, D., Fetters, L., Dounis, P. & Lovegrove, R. (2000). *Energy Fuels*, **14**, 419–430.
Loo, Y. L., Register, R. A., Ryan, A. J. & Dee, G. T. (2001). *Macromolecules*, **34**, 8968–8977.
Mandelkern, L. (2004). *Physical Properties of Polymers*, edited by J. E. Mark. Cambridge: University Press.
Mckenna, T. F. (1998). *Eur. Polym. J.* **34**, 1255–1260.
Murthy, N. S., Akkapeddi, M. K. & Orts, W. J. (1998). *Macromolecules*, **31**, 142–152.
Murthy, N. S., Stamm, M., Sibilia, J. P. & Krimm, S. (1989). *Macromolecules*, **22**, 1261–1267.
Paricaud, P., Galindo, A. & Jackson, G. (2004). *Ind. Eng. Chem. Res.* **43**, 6871–6889.
Rogers, C. E., Stannett, V. & Szwarc, M. (1959). *J. Phys. Chem.* **63**, 1406–1413.
Schelten, J., Ballard, D. G. H., Wignall, G. D., Longman, G. & Schmatz, W. (1976). *Polymer*, **17**, 751–757.
Schmidtke, J., Strobl, G. & Thurn-Albrecht, T. (1997). *Macromolecules*, **30**, 5804–5821.
Stamm, M., Fisher, E. W., Dettenmaier, M. & Convert, P. (1979). *Faraday Discuss.* **68**, 263–279.
Weinkauf, D. H. (1990). *Barrier Polymers and Structures*, edited by W. J. Koros, Vol. 423, ch. 3. Washington, DC: American Chemical Society.
Wignall, G. D. (2004). *Physical Properties of Polymers*, edited by J. E. Mark. Cambridge University Press.